The Prediction of Vortex Interactions on a Generic Missile Configuration Using CFD: Current Status of Activity in NATO AVT-316

N. Taylor
MBDA UK
GBR
nigel.j.taylor@mbda-systems.com

G. McGowan, M. Anderson
Corvid Technologies
USA

C. Schnepf, K. Richter
German Aerospace Center (DLR)
DEU

M. Tormalm
Swedish Defence Research Agency (FOI)
SWE

G. Loupy, V. Michel, C. Jeune
MBDA F
FRA

S. Shaw
MBDA UK
GBR

E. Dikbaş
TÜBİTAK SAGE
TUR

G. Barakos, K. Boychev
University of Glasgow
GBR

C. Toomer
University of the West of England
GBR

J. DeSpirito
U.S. Army Research Laboratory
USA

ABSTRACT

This paper provides a brief overview of the activities undertaken by the Missile Facet of NATO STO AVT 316 (Vortex Interaction Effects Relevant to Military Air Vehicle Performance) since its first meeting in April 2018. Rather than setting out to provide definitive technical statements, a broader, more narrative approach is taken towards summarising some of the key developments that have occurred during the early stages of the facet's existence. To date, work has focussed on investigating a blind test case (CFD_OTC1) based on a generic missile airframe at a supersonic flight condition. Attention is focussed on the predicted total rolling moment coefficient, the polarity of which determines the airframe's local static roll stability. While the facet

is still some way from demonstrably achieving verified CFD solutions at the flight condition of primary interest, there is now little doubt that the airframe will be predicted to be locally unstable in roll.

1.0 INTRODUCTION

The manoeuvrability and agility of missiles require the controlled exploitation of complex, vortex-dominated flows. These may incorporate multiple close-proximity vortex interactions, between vortices, vortices and airframe components, and vortices and shock waves. Requirements to reduce (a) development costs and (b) time-to-theatre are leading to a stronger reliance on computational modelling & simulation (and a reduced reliance on physical testing) to support missile design and performance assessment. Consequently, there is increasing interest in using Computational Fluid Dynamics (CFD) to predict these challenging flows and to do so at an early stage in the product development lifecycle (thereby also reducing dependencies on simpler, semi-empirical prediction techniques). This poses the practising industrial missile aerodynamicist with a variety of challenges and dilemmas. Reviewed further in [1], these ultimately stem from the recognition that reliable solutions of the (complete) Navier-Stokes equations for such flows are not currently available and that the consequences of computational modelling simplifications are generally not readily quantifiable *a priori*.

In January 2018, AVT-316 (Vortex Interaction Effects Relevant to Military Air Vehicle Performance) was established. The Task Group was split into two facets: an Aircraft Facet and a Missile Facet, each focussing on the vortex interactions associated with airframes of direct interest to NATO. In particular, the Missile Facet was established to:

- Assess the current capabilities of CFD to predict missile aerodynamic characteristics for flows containing multiple vortex interactions
- Share and seek to learn from comparable experience of applying CFD to other classes of NATO vehicles (combat aircraft, in particular)
- Consolidate lessons learned and any attendant future requirements

This paper provides a brief overview of the activities undertaken by the Missile Facet since its first meeting in April 2018. Rather than setting out to provide definitive technical statements, a broader, more narrative approach is taken towards summarising some of the key developments that have occurred during the early stages of its existence. This stance has been adopted for several reasons. The findings and insights gained to date are not considered to be mature – indeed, much of the material presented is rather fresh and has not yet been subjected to detailed, systematic analysis or scrutiny. The intent is to convey some of the diversity and complexity of the issues that may be faced on a daily basis when applying CFD to predict the aerodynamic characteristics of missiles and to provide an indication of the scope and scale of effort required to build confidence in the bounds of uncertainty that should be applied to CFD predictions. A more detailed and definitive record of the Missile Facet's activity will be produced at a later date.

The test case developed for the facet, CFD_OTC1, and the approach taken towards its use are described in Section 2. Section 3 outlines the initial results obtained for CFD_OTC1 by the facet members. Sections 4 and 5 review the data that have been obtained to date in studies motivated by these original findings, distinguishing between those involving steady and unsteady simulations, respectively. Section 6 provides some closing remarks and pointers as to where the facet is heading next.

2.0 APPROACH

The Missile Facet activity described in this paper has focussed on a blind test case – one for which no

physical test data exists. This decision was made intentionally, partly to reflect the situations encountered during the early stages of the product development cycle (i.e. prior to wind tunnel testing having taken place). For the reasons explained below, an additional intent was to deliberately expose some of the challenges faced in arriving at a suitably verified CFD solution – a pre-cursor of any validation activity.

2.1 The CFD_OTC1 Test Case

The missile airframe used as the basis for the CFD_OTC1 Test Case possesses a simple axi-symmetric body, four low aspect ratio wings and four tail control fins in a classical cruciform layout. Its Outer Mould Lines (OML) are illustrated in Figure 24-1. The corresponding axes systems and wing/fin numbering conventions are presented in Figure 24-2. The Missile Body Axes (MBA) are right-handed orthogonal, with rotations and moments being positive clockwise when viewed along the axis of rotation in the positive sense from the origin, which is located on the centreline at 50% of the body length.

Figure 24-1: Outer mould lines of the CFD_OTC1 generic missile airframe

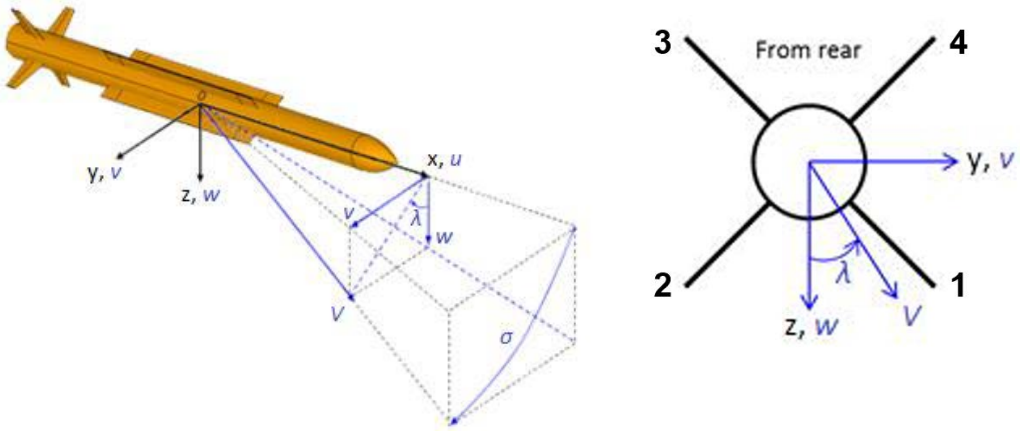

Figure 24-2: Missile Body Axes and wing/fin numbering conventions

The flight condition of primary interest was as follows: Mach number: 1.4; Reynolds number (based on the missile base diameter, d_{Ref}): $4.89*10^6$; Total Incidence (σ): 15.0° and Aerodynamic Roll Angle (λ): 2.5°; where $\cos(\sigma) = u/V$, $\tan(\lambda) = v/w$, $V^2 = u^2 + v^2 + w^2$ and V is the total missile linear velocity with respect to the freestream.

Overall aerodynamic force and moment coefficients, defined in MBA and denoted as C_X, C_Y, C_Z, C_l, C_m and C_n (where l, m and n are the moments about the x-, y- and z-axes, respectively), were defined as follows: (using X and m as examples of the total aerodynamic force and moments):

$$C_X = \frac{X}{q_\infty S_{\text{Ref}}} \text{ and } C_m = \frac{m}{q_\infty S_{\text{Ref}} d_{\text{Ref}}}$$

where q_∞ is the freestream dynamic pressure and the reference area, S_{Ref} is ($\pi d_{Ref}^2/4$).

This flight condition was selected on the basis of past experience of applying CFD to similar airframe configurations where, when seeking steady solutions of the Reynolds-Averaged Navier-Stokes (RANS) equations, difficulties demonstrating predictable dependencies on mesh resolution had been encountered. The computed results could also be sensitive to the chosen modelling approach, for example the choice of turbulence model or whether the flow was modelled as being steady or unsteady. A particular metric of interest here was the total rolling moment coefficient, C_l, the sign (polarity) of which could change depending on the assumptions made during the computation. The practical significance of this being that the airframe could be predicted to be either locally statically stable in roll (if the value of C_l was negative) or unstable (if positive).

2.2 The AVT-316 Missile Facet

The current membership of the AVT-316 Missile Facet is captured in this paper's list of authors. While limited (from the viewpoint of conducting statistical analyses of the results) in its number of participating organisations, the facet has a broad membership – encompassing industrial organisations, government agencies, research establishments and academia – and brings to bear a healthy blend of experienced CFD users and code developers. The range of CFD tools used by the facet to-date, is summarised in Table 1.

Table 24-1: The CFD tools used to-date by the AVT-316 Missile Facet

ORGANISATION	MESH GENERATION SOFTWARE	FLOW SOLVER
CORVID Technologies	Pointwise[2]	RavenCFD[3]
DLR	CENTAUR[4]	TAU[5]
FOI	ICEMCFD[6] (surface), TRITET[7] (volume)	M-Edge[8]
MBDA F	ANSA[9]	FLUSEPA[10]
MBDA UK	SOLAR[11]	TAU[5]
TÜBİTAK SAGE	ANSYS Meshing[12] (surface), TGRID[13] (volume)	FLUENT[14]
Univeristy of Glasgow	ICEMCFD[6]	HMB3[15]
US Army Research Laboratory	CAPSTONE[16]	CFD++[17], KESTREL[18]

3.0 INITIAL ACTIVITY AND FAMILIARISATION

In order to allow Missile Facet members to become familiar with the CFD_OTC1 Test Case and also to act as a baseline by which to judge subsequent progress, all facet members were required to compute the overall aerodynamic force and moment characteristics at the flight condition described in Section 2.1, above (subsequently referred to as the mandatory flow condition) and to demonstrate the sensitivity of their approach to mesh resolution. Other than the material described in Section 2.1, the only information provided was a boundary representation (BREP) of the OML (via a STEP file). Members were free to choose whatever they wished as to how the flow solutions were obtained – e.g. mesh type, numerical scheme, turbulence model, etc. They were also allowed to decide which form of governing equations to solve – although, for simplicity, members were asked to assume that boundary layers were fully turbulent.

These initial computations generated a wealth of information. Paper length constraints dictate that only a very limited amount can be re-produced herein. A summary of the initial results obtained is presented in Figure 24-3. This shows a series of mesh convergence histories for the total rolling moment coefficient, C_l – the coefficient that exhibited the most irregular sensitivity to mesh resolution. Data is presented in two ways: C_l is plotted against (a) N, the number of degrees of freedom afforded in the flow solver by the mesh, i.e. the number of mesh nodes (for node-centred flow solvers), number of cells (for cell-centred schemes) and (b) $N^{-2/3}$, a parameter widely used to assess mesh convergence for second-order numerical schemes. Note that since the HMB3 code uses a 3rd order scheme, these data have been removed from this part of the Figure. (This also allowed the trends exhibited by the RANS data to be made more discernible.)

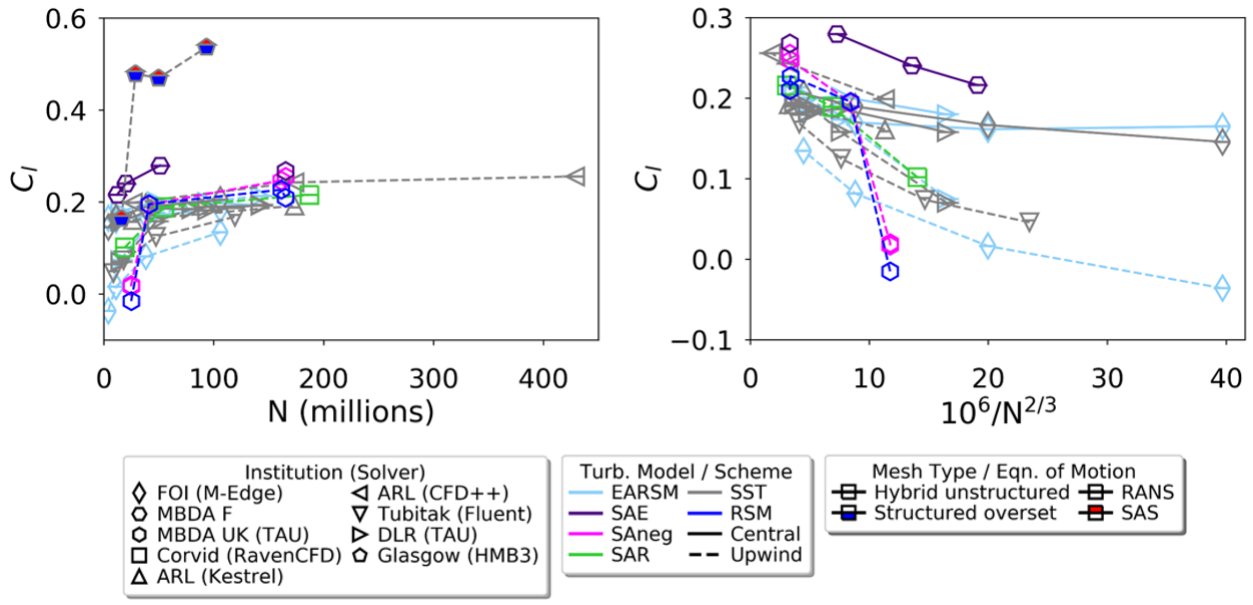

Figure 24-3: A selection of the initial total rolling moment coefficient data computed for the mandatory flow condition

The following observations concerning the data presented in Figure 24-3 are considered to be the most salient at this stage of the paper's narrative:

(i) Although there are two examples of the computed rolling moment being negative, these results (and other similar outcomes, not reported here) were obtained for relatively coarse meshes: most of the reported data indicate the airframe is locally unstable in roll.

(ii) While the RANS solutions generally appear to be approaching, in the limit, values above 0.2, there is a large percentage variance in the different sets of results. Considerable differences in trend are also evident: for instance, while most sets of data exhibit regular patterns of monotonic convergence, this is not true of all of them.

(iii) Results obtained using Scale Adaptive Simulation (SAS), on structured overset meshes, differ markedly from those obtained using RANS on hybrid unstructured meshes and indicate a far more unstable airframe.

Another perspective on the initially observed mesh sensitivity is provided in Figure 24-4. This presents a series of total pressure ratio ($p_0/p_{0,\infty}$) contour plots, evaluated in a cross-flow plane at an axial station corresponding to the 50% fin-chord line (21.5 base diameters aft of the nose apex), for a fixed set of RANS modelling assumptions. Data for four hybrid, unstructured meshes are presented. Focussing for the time being on two of the vortex cores evident in the Figure (those close to the tips of Fins 3 and 4), their resolution is clearly improved with each refinement of the mesh. Their locations with respect to the fins are also affected. On further inspection of the computed flowfields and the aerodynamic load distributions on the airframe, these factors appear to be the dominant sources of the variation in total rolling moment coefficient seen in Figure 24-3. However, a degree of caution should be expressed here, since the computed flowfields are extremely complex and exhibit multiple physical phenomena and closely coupled interactions thereof, each of which will be contributing to the overall effect. Figure 24-5 identifies the principal off-surface and surface flow features.

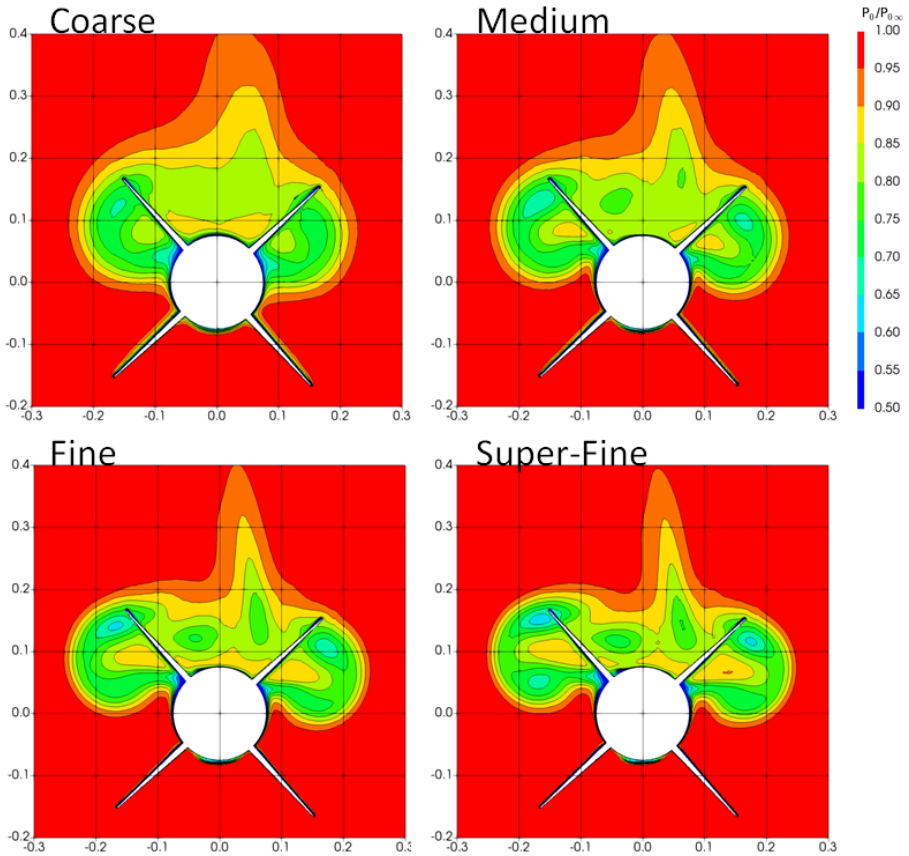

Figure 24-4: An example of the effect of mesh resolution on total pressure ratio evaluated at fin mid-chord for the mandatory flow condition (View from the rear of the missile) [Source: FOI/M-Edge, RANS, 2nd order upwind (minmod limiter), EARSM; N (millions) = 4 (Coarse), 11.2 (Medium), 38.3 (Fine), 106 (Super-Fine)]

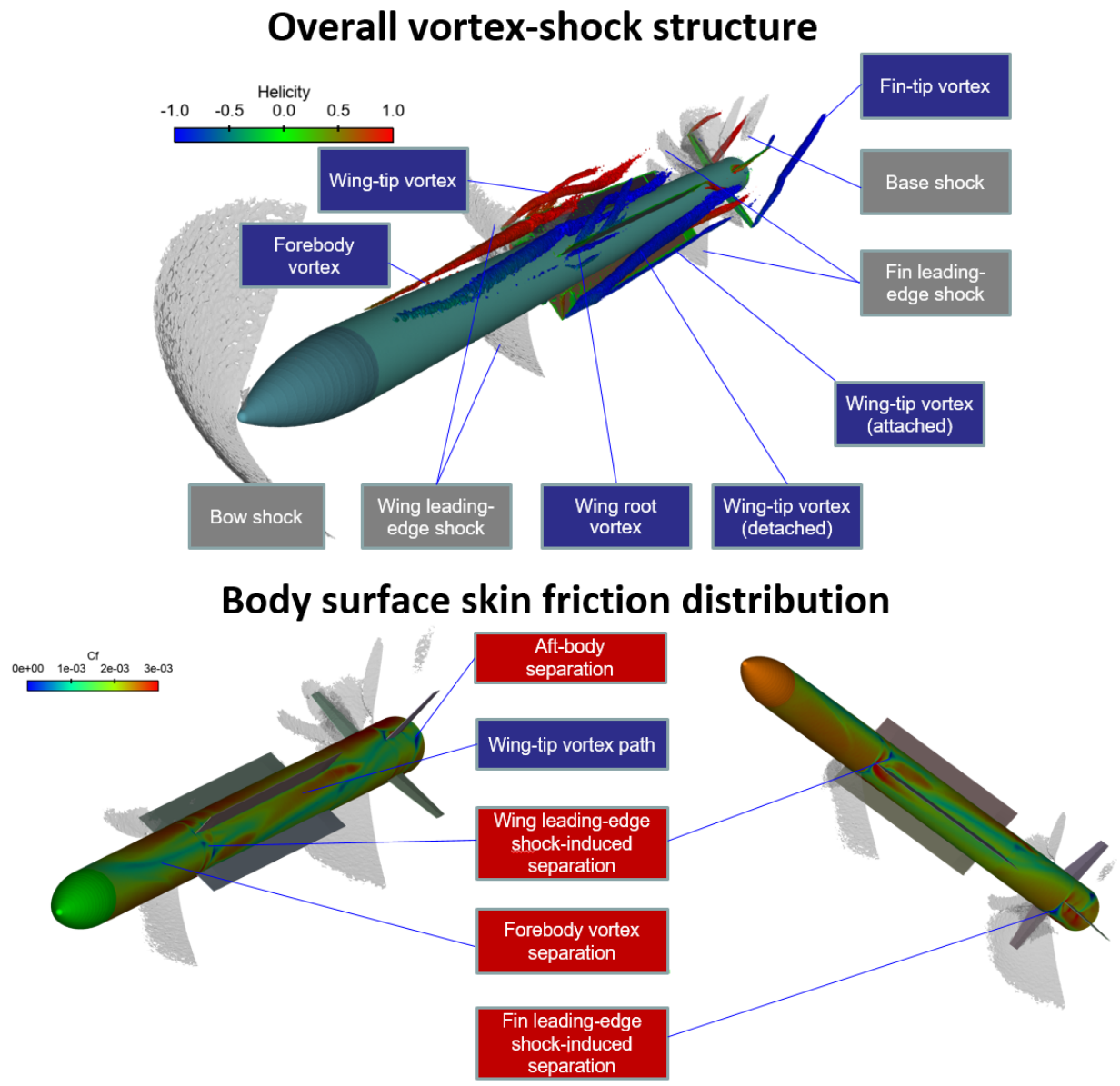

Figure 24-5: The principal off-surface and surface flow features at the mandatory flow condition [Source: TÜBİTAK SAGE/FLUENT, RANS, 2nd order upwind (minmod-based limiter), SST; N = 47 million]

Inspection of the computed flowfields indicated differing levels of dissipation in the definition of the vortices interacting with Fins 3 and 4. As Figure 24-6 illustrates, this dissipation was most pronounced in the solutions obtained on the coarsest meshes; the choice of central or upwind numerical scheme also appeared to have an influence. These observations formed the initial stimuli for subsequent investigations.

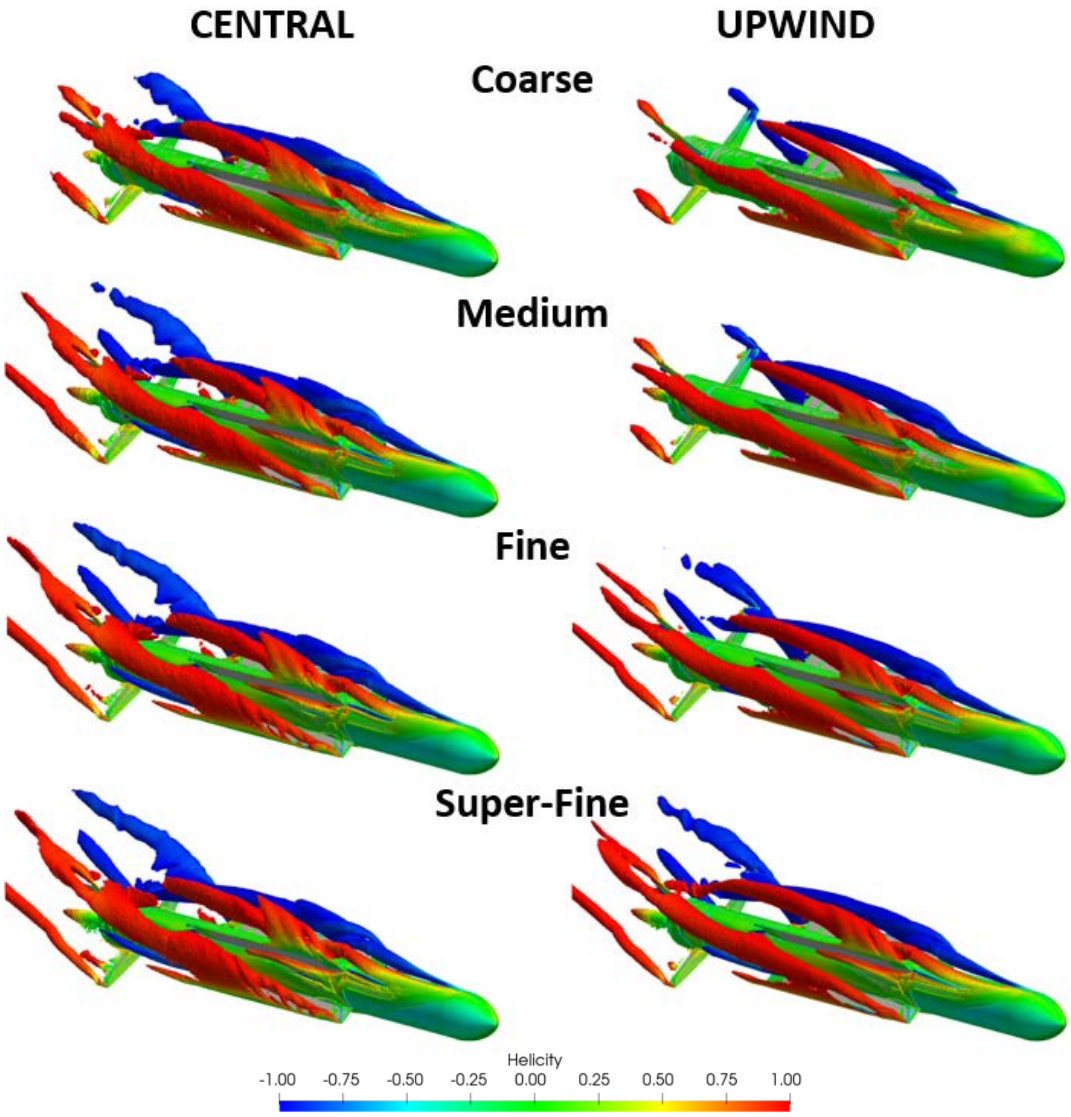

Figure 24-6: The influence of mesh resolution and numerical scheme on the levels of dissipation evident in the vortices ahead of Fins 3 and 4 for the mandatory flow condition [Source: as per Figure 24-4]

Again, in view of the diversity of factors that could be investigated, together with the breadth of experience in the facet, facet members were encouraged to follow their experience and judgement rather than a strict, pre-defined and closely co-ordinated study plan. Consequently, several activities were pursued more-or-less in parallel. However, as a result of the strong interactions within the facet, few were pursued in isolation. For convenience, the results are reviewed under two broad headings below: those associated with RANS computations (Section 4) and those in which the flow was permitted to be unsteady (Section 5).

4.0 SUBSEQUENT RESULTS: RANS

Some of the key outcomes from the RANS investigations are outlined under four headings: (i) Roll Angle Effects; (ii) The Effect of Limiters; (iii) Increasing the Order of the Turbulent Flux Reconstruction Scheme and (iv) The Influence of Volume Mesh Topology.

4.1 Roll Angle Effects

In order to gain a better appreciation of the factors governing the sensitivity of the results to aerodynamic roll angle, two lines of investigations were followed. One was primarily interested in assessing how the aerodynamic loading acting on Fins 3 and 4 is affected by roll angle. The other was primarily concerned with understanding whether the mesh dependencies observed at λ=2.5° were encountered at other roll angles.

Figure 24.7 presents a sequence of total pressure ratio contour plots at the fin mid-chord station for aerodynamic roll angles ranging from 0° to 5°. The symmetry of the flowfield at λ=0° indicates that the rolling moment computed at λ=2.5° is not a consequence of the formation of asymmetric forebody vortices. As the roll angle increases, a progressive weakening and translation of the vortex core beneath the tip of Fin 4 away from the fin is apparent. In conjunction with the strengthening and restrained movement of the corresponding vortex passing Fin3, together with the attendant trends in the loads acting on each fin, these observations provided further justification for focussing interest on these vortex interactions.

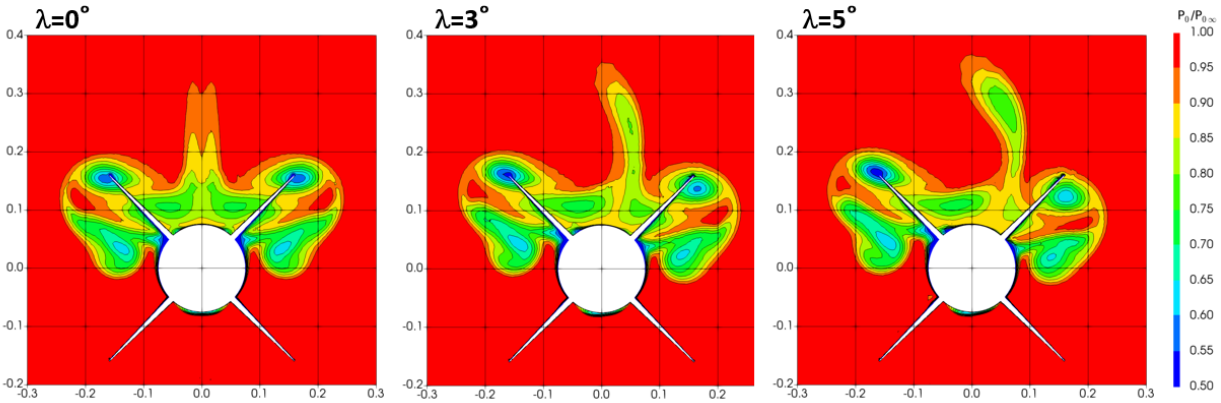

Figure 24-7: Evolution of the vortex interactions with Fins 3 and 4 with aerodynamic roll angle at fin mid-chord (View from the rear of the missile)
[Source: MBDA F, RANS, 2nd order central, SA; N = 32million]

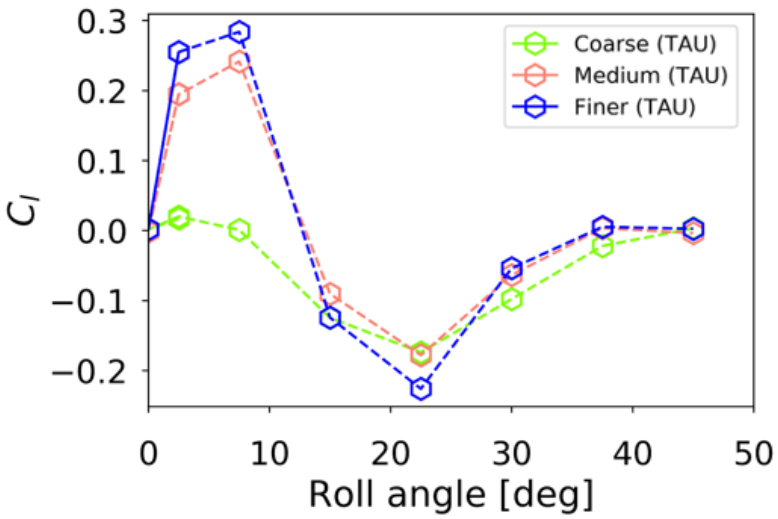

Figure 24-8: Sensitivity of total rolling moment coefficient to hybrid unstructured mesh resolution as a function of aerodynamic roll angle
[Source: MBDA UK/TAU, RANS, 2nd /1st order upwind (TAU standard limiter), SA-neg; N (millions) = 24.8 (Coarse), 41.1 (Medium), 165.2 (Finer)]

Given the proximity of these vortices to the tips of these fins, it is not particularly surprising that the computed rolling moments are so sensitive to the mesh resolution. Figure 24-8 indicates that, for hybrid unstructured meshes, a similar level of mesh sensitivity may persist out to roll angles up to about 15° (i.e. ~33% of the maximum operational roll angle range). Despite the potential implications for local airframe roll stability, no further investigations of the mesh sensitivity at roll angles other than 2.5° have been undertaken to-date.

4.2 The Effects of Limiters

In view of the increased dissipation evident in the results obtained using upwind schemes (see Figure 24-6), an investigation into the effects of limiters was undertaken. The total rolling moment coefficients obtained using a range of limiters on the same hybrid unstructured mesh are presented in Figure 24-9. The variation in C_l was found to be larger than that associated with the choice of turbulence model (SARC, SST-RC) on that mesh – and broadly comparable with that evident in Figure 24-3 for similar values of N. The values of C_l obtained with the more dissipative limiters were lower than those produced using limiters considered to be less dissipative.

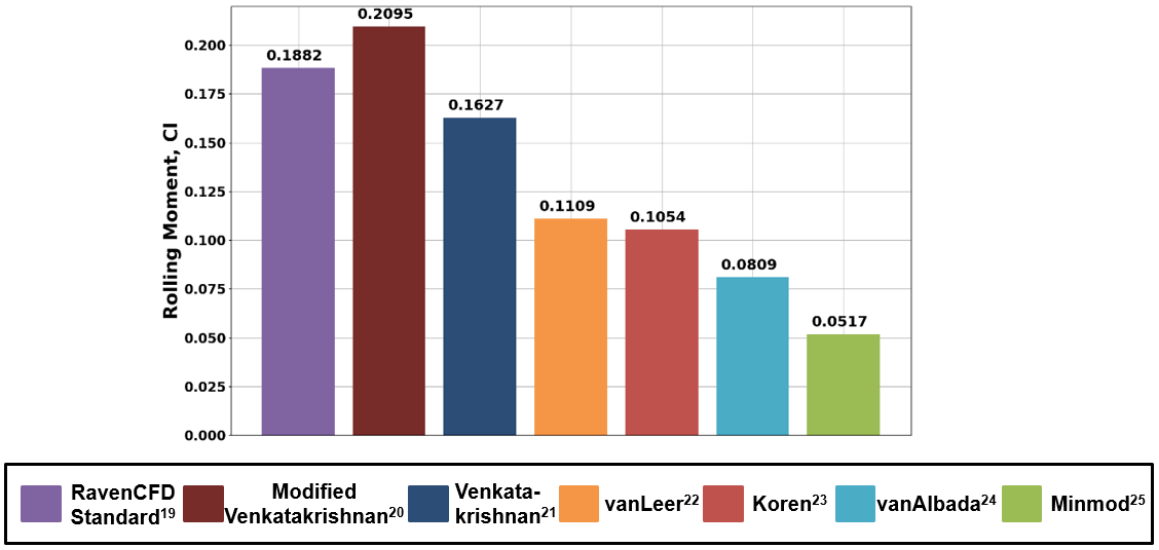

Figure 24-9: The sensitivity of total rolling moment coefficient to choice of limiter when using an upwind scheme on a hybrid unstructured mesh (N = 55 million) [Source: Corvid/RavenCFD, RANS, 2nd order upwind, SAR]

An investigation of the computed flowfields associated with the data presented in Figure 24-9 indicated that the choice of limiter had a strong effect on the trajectories and intensity of the vortices shed from Wings 1 and 2 on their passage towards Fins 4 and 3, respectively. Figure 24-10 summarises this by comparing contours of Q criterion at the fin mid-chord station. It is apparent that the limiters producing the larger values of C_l in Figure 24-9 are also those that yield larger vortices that pass closer to the fins.

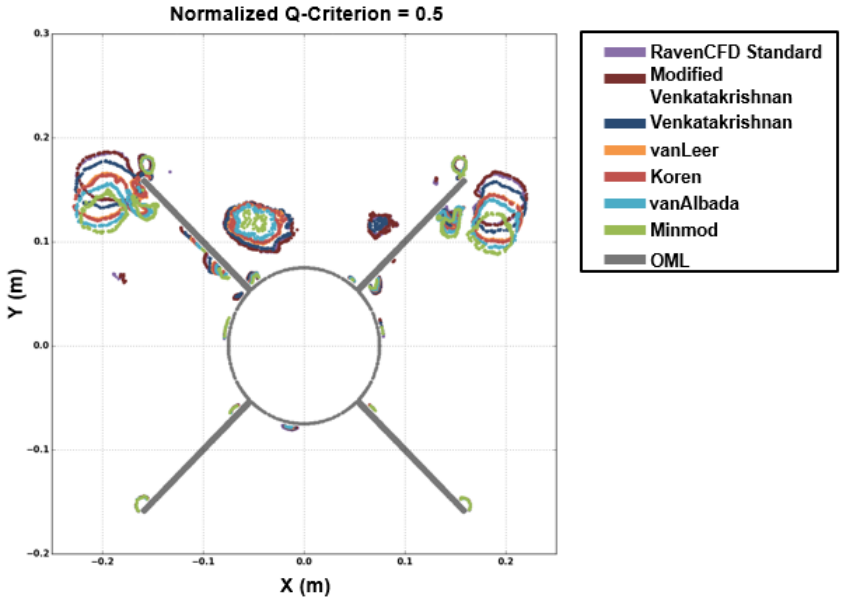

Figure 24-10: The effect of choice of limiter on normalized Q criterion at the fin mid-chord station when using an upwind scheme on a hybrid unstructured mesh (View from rear of the missile) [Source: Corvid/RavenCFD, RANS, 2nd order upwind, SAR; N = 55 million]

The effects of the choice of limiter were studied further using the simple, isolated isentropic vortex test case described in [26]. Results were obtained for unstructured and structured meshes of varying spatial resolution: the number of cells on each side of the rectangular far-field boundary was varied from 100 to 400. The results, in the form of radial distributions of static pressure ratio (p/p_∞), are summarised in Figure 24-11. This shows that the errors in static pressure throughout the vortex core could be substantial and that it only proved possible to approach their elimination on the finest structured mesh studied. Although it is difficult to make direct comparisons between this test case and CFD_OTC1, judging from the number of cells spanning the largest Q-criterion contours in Figure 24-10, (~18), the local spatial resolution afforded by the mesh was somewhere between that afforded by the Coarse and Medium meshes of Figure 24-11 – all of which yielded appreciable discretisation error, regardless of the limiter used.

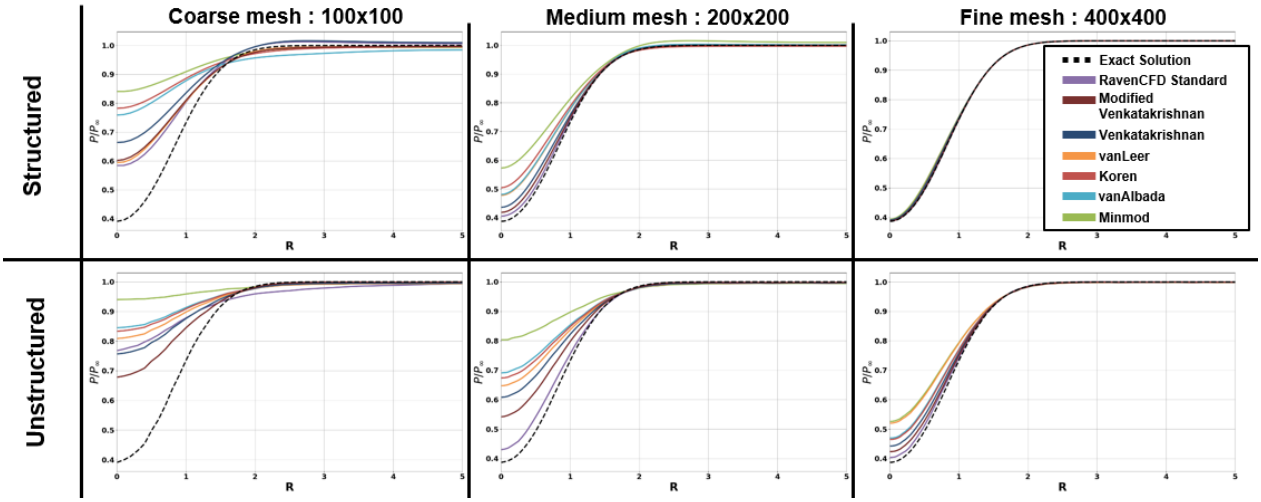

Figure 24-11: The effect of choice of limiter on the radial distribution of static pressure ratio computed about a simple, isolated isentropic vortex, for various structured and unstructured meshes [Source: Corvid/RavenCFD, RANS, 2nd order upwind, SAR]

4.3 Increasing the Order of the Turbulent Flux Reconstruction Scheme

In order to improve the overall robustness of turbulent computations, some solvers allow users to select a first-order discretization of the fluxes associated with the turbulence model equations. In order to understand the impact of this choice on the accuracy of the mean flow computation, TAU calculations were performed with first- and second-order discretizations of the turbulence model equations. In both instances the mean flow equations were discretized with a second-order scheme. The results, summarised in Figure 24-12, show that the use of higher order schemes for the convective turbulent fluxes yielded appreciable increases in the computed total rolling moment coefficient. Indeed, values of C_l in excess of those obtained previously from any computation were produced. This work included initial investigations into the use of a different type of hybrid unstructured volume mesh – one which made greater utilisation of hexahedral cells (and is herein referred to as Hybrid "Type B") – as described in Section 4.4, below.

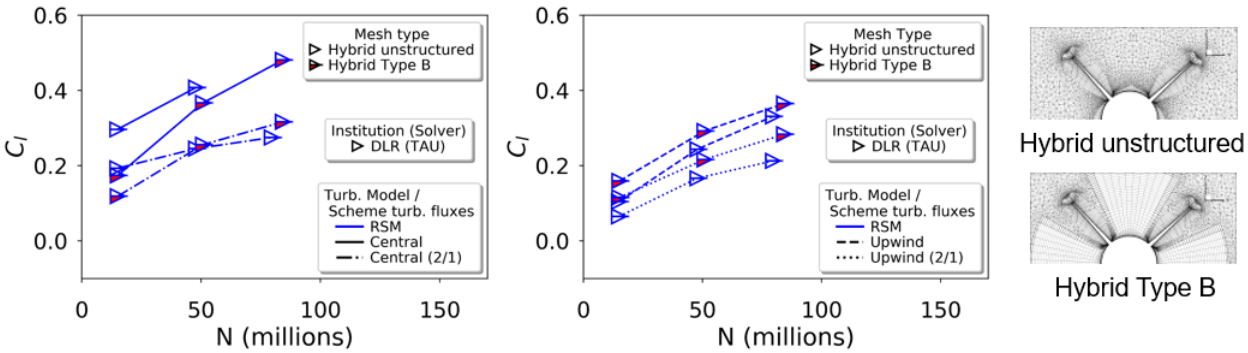

Figure 24-12: The influence of convective turbulent flux scheme order and mesh topology on the total rolling moment coefficients computed by TAU

4.4 The Influence of Volume Mesh Topology

Following the results described in Sections 4.2 and 4.3, the effects of using a hybrid overset mesh (built using an unstructured surface mesh and a prismatic layer mesh, and a more highly resolved structured background mesh) were compared with those obtained using a more classical hybrid unstructured mesh and the finest available mesh possessing a hybrid "Type B" topology using RavenCFD (a cell-centred solver). The three volume meshes included in this comparison are illustrated in Figure 24-13. Note that the total number of cells in the hybrid overset mesh was broadly similar to that in the hybrid unstructured mesh, but substantially less than the number in the hybrid Type B. The corresponding total pressure contours at fin mid-chord are compared in Figure 24-14.

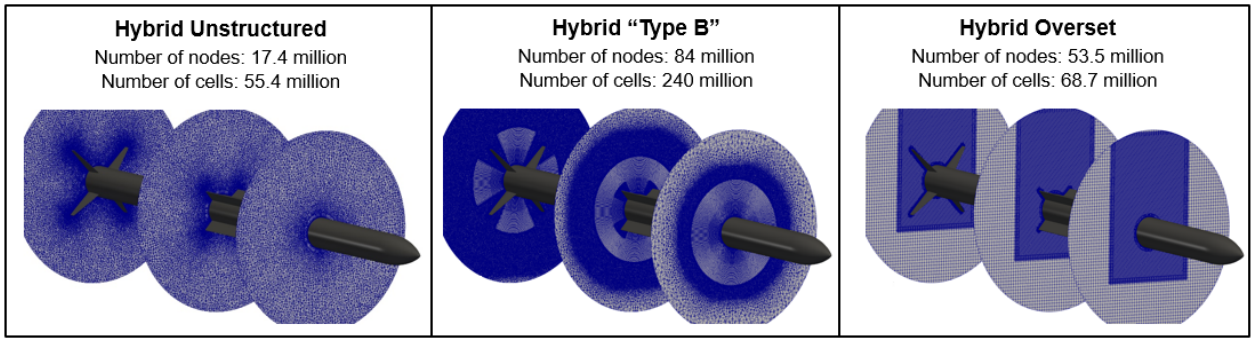

Figure 24-13: The three types of volume mesh topology included in the current study

In spite of the aforementioned trends in total cell count, the hybrid overset mesh appeared to produce the most detailed resolution of the flow features at this station and, simultaneously, yielded the highest total rolling moment coefficient. No further attempts have yet been made to further improve the efficiency of the Type B hybrid mesh.

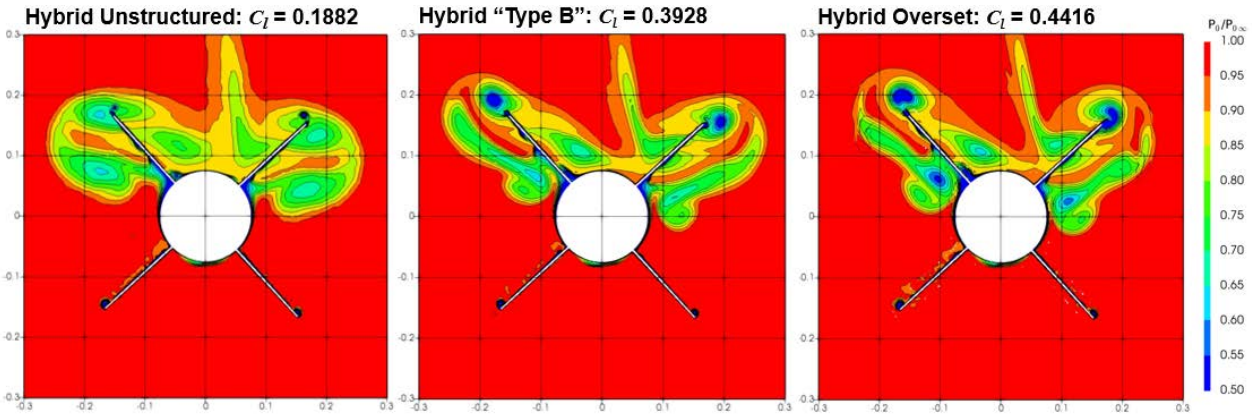

Figure 24-14: Comparison of results obtained at the fin mid-chord station for the meshes illustrated in Figure 24-13 (View from rear of the missile)
[Source: Corvid/RavenCFD, RANS, 2nd order upwind (RavenCFD standard limiter), SAR]

5.0 SUBSEQUENT STUDIES: UNSTEADY FLOW SIMULATIONS

In response to the distinctly different values of total rolling moment coefficient obtained using SAS compared with RANS (Figure 24-3), together with the expectation that, because of the large regions of separated flow present, seeking a steady solution might not be the most appropriate approach to take, several facet members started to look at unsteady flow solutions, via Detached Eddy Simulation (DES), Delayed Detached Eddy Simulation (DDES) or Improved Delayed Detached Eddy Simulation (IDDES). The mean values of the computed total rolling moment coefficients for these unsteady computations are presented alongside the results obtained using RANS in Figure 24-15.

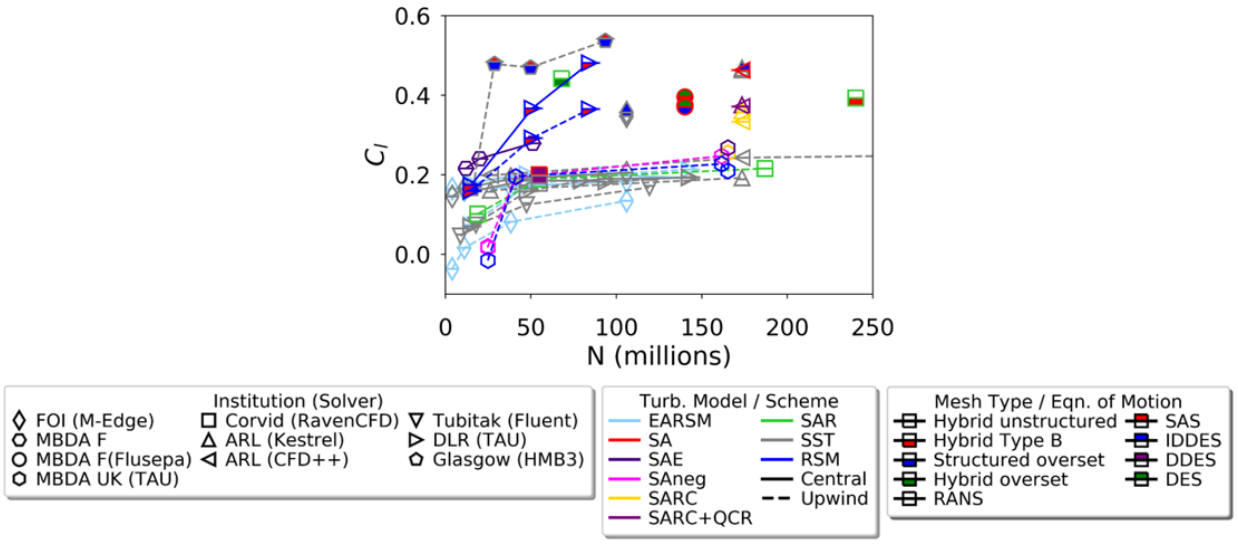

Figure 24-15: Summary of the total rolling moment coefficient data computed to-date for the mandatory flow condition (further details are provided in Figure 24-17)*

* Key to turbulence model abbreviations used herein: SA: Spalart-Allmaras; SARC: Spalart-Allmaras with Rotation/Curvature Correction; SARC+QCR: Spalart-Allmaras with Rotation/Curvature Correction and Quadratic Constitutive Relation; SAR:

While the original SAS data no longer look like outliers in quite the same way – either with respect to the other unsteady data or the latest RANS results – the recent unsteady data has done nothing to improve the situation regarding mesh sensitivity. (Although this situation is clouded somewhat by the fact that refining a mesh in unsteady flow simulations also alters the balance between the frequency content that is resolved and that which is modelled.)

As expected, the most highly resolved and higher order unsteady computations also identified details in the flow that were not previously evident in the RANS results. This may be seen by comparing Figures 24-6 and 24-16. For instance, a shear layer swirling around the core of the vortex shed from each wing tip is now apparent. This shear layer appears to breakdown ahead of the fins, creating more complex and dynamic structures around the vortex cores.

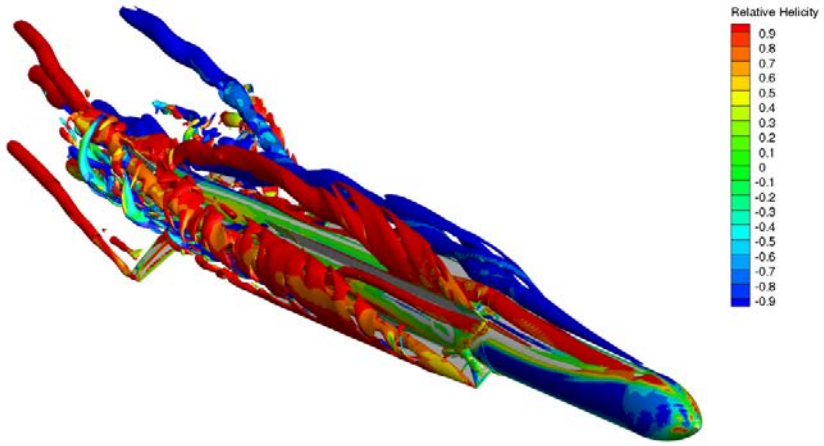

Figure 24-16: Instantaneous Q-criteria iso-surfaces, coloured with relative helicity [Source: MBDA F/FLUSEPA, DES, 4th order central, explicit dt ~ 8.6x10^{-7}s]

Although a number of solution options (e.g. spatial order, numerical scheme and timestep) have been explored, Figure 24-17 (which presents time histories of the computed total rolling moment coefficient) shows that we are still some way from achieving spatial and temporal solution convergence. Moreover, unsteadiness in the total rolling moment coefficient only becomes apparent in the more finely resolved solutions.

Spalart-Allmaras with Rotation Correction; SAE: Spalart-Allmaras with Edwards modification; SAneg: Negative Spalart-Allmaras; EARSM: Explicit Algebraic Reynolds Stress Model; SST: Menter's Shear Stress Transport model; RSM: SSG/LRR Reynolds Stress Model

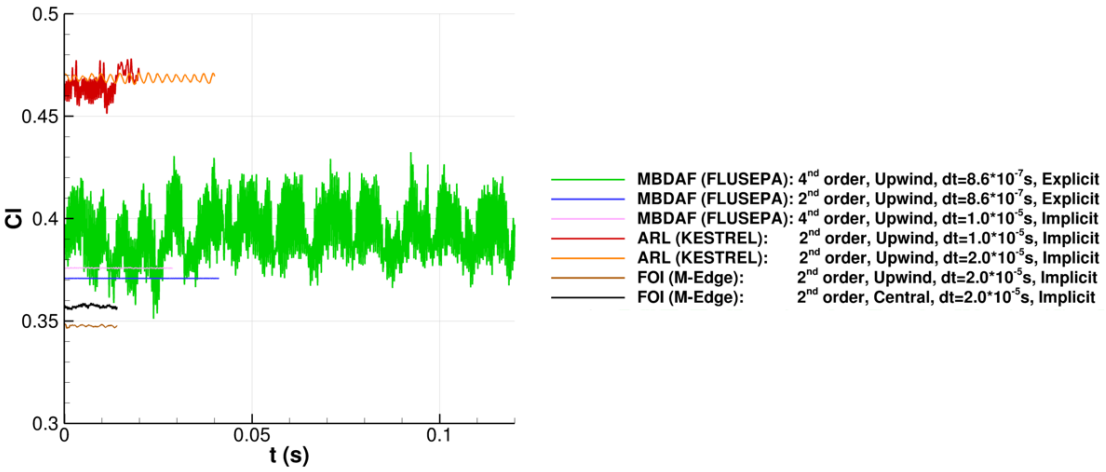

Figure 24-17: A selection of total rolling moment coefficient time histories obtained from unsteady computations

Investigating this issue further will have increasing implications for cost: not just in solving the governing equations, but also in terms of the elevated resources required for post-processing the results. With this in mind, it is noteworthy that initial investigations into the sensitivity of the computed overall aerodynamic forces and moments to Reynolds number have indicated that the Reynolds number could be reduced by as much as 50% without having a large effect on the results. Since the Reynolds number specified in Section 2.1 corresponds to a full-scale missile flying in International Standard Atmosphere sea level conditions, reductions in computational costs could be sought by simulating the flow generated by a sub-scale airframe, representative of that which might be tested in a wind tunnel, for instance. However, this possibility has not yet been explored.

6.0 CLOSING REMARKS

By providing a broad narrative of the ways in which the work of the Missile Facet has evolved during the first eighteen months of its existence, this paper has provided some insights into the scope and complexity of the challenges that can be faced by users of contemporary CFD codes in securing verified solutions. In this regard, the benefits of community benchmarking have been keenly felt throughout the facet. Nevertheless, we are still some way from reducing the various contributions to discretisation error to the point at which the effect of other modelling assumptions – the choice of turbulence model, for instance – can be studied reliably.

In order to provide some balance to what might otherwise be viewed as an inconclusive situation, there is now little doubt that the airframe will be predicted to be locally unstable in roll at the mandatory flow condition. Moreover, while the potential uncertainty in the predicted value of total rolling moment coefficient is currently quite large when expressed as a percentage of the mean, it is appreciably smaller than that which would be expected from semi-empirical predictions unless such predictions had been tuned specifically for this particular class of flows. Indeed, for many semi-empirical tools, predictions for cruciform airframes are derived only from data at roll angles of 0°, 22.5° and 45°. So, in these cases, prediction of this type of local roll instability is fundamentally beyond their scope.

As may be judged from the manner in which the material has been reported, the situation regarding solution verification is fairly dynamic, with interesting developments still occurring more-or-less on a monthly basis.

Looking forwards, aside from pursuing the topics described above further, several additional investigations are either underway or planned. These will include exploratory applications of adaptive mesh refinement and more formal assessments of mesh convergence. More detailed analyses of the physical properties of the vortices and their interactions are also planned. It is intended to conclude this part of the facet's work by repeating the initial analysis (summarised in Section 3) in a more controlled and systematic way, making use of the lessons learned to date. The intent is to produce a more definitive and detailed record of the facet's study of the CFD_OTC1 Test Case, including a consolidated set of recommendations, at a later date.

REFERENCES

[1] Taylor, N.J., "Separated Flow: Some Challenges and Research Priorities for Missile Aerodynamics", STO-MP-AVT-307-23, 2019.

[2] Pointwise, Version 18, Pointwise, Inc., Fort Worth, TX, 2019.

[3] RavenCFD, Version 4.503, Corvid Technologies, Mooresville, NC, 2019.

[4] CENTAUR, CENTAUR Software, https://www.centaursoft.com/

[5] Schwamborn, D., Gerhold, T. and Heinrich, R., "The DLR TAU-Code: Recent applications in research and industry", Invited Lecture in "Proceedings on CD of the European Conference on Computational Fluid Dynamics ECCOMAS CFD 2006", P. Wesseling, E. Oñate and J. Périaux (Eds), The Netherlands, 2006.

[6] Tysell, L., "The TRITET Grid Generation System". Proceedings of the 10th ISGG Conference on Numerical Grid Generation, Forth, Crete, Greece 2007.

[7] ANSYS ICEM CFD Programmer's Guide (Release 17.2), ANSYS, Inc., 2016.

[8] Eliasson, P., "Edge, a Navier-Stokes solver for unstructured grids", Proc. To Finite Volumes for Complex Applications III, ISBN 1 9039 9634 1, pp.527-534, 2002.

[9] ANSA, Version 19.1.0, BETA CAE Systems, Switzerland, 2019.

[10] Pont, G., "Self adaptive turbulence models for unsteady compressible flows", PhD Thesis, ENSAM, April 2015.

[11] Martineau, D.G., et al., "Anisotropic hybrid mesh generation for industrial RANS applications", AIAA 2006-534, January 2006.

[12] ANSYS Meshing User's Guide (Release 15.0), ANSYS Inc., 2013.

[13] ANSYS Fluent Meshing (TGrid) User's Guide (Release 15.0), ANSYS Inc., 2013.

[14] ANSYS Fluent User's Guide (Release 14.0), ANSYS Inc., 2011.

[15] Lawson, S. and Barakos, G., "Review of Numerical Simulations For High-Speed, Turbulent Cavity Flows," Progress in Aerospace Sciences, Vol. 47, No. 3, pp. 186 – 216, 2011.

[16] Mestreau, E. et al., CAPSTONE "CREATE-MG Capstone: Design, Architecture & Feature Modelling

Improvements", AIAA-2019-1716, January 2019.

[17] CFD++ Version 18.1 User Manual, Metacomp Technologies, Inc., Agoura Hills, CA, 2018.

[18] McDaniel, D. R. and Tuckey, T. R., "HPCMP CREATETM-AV Kestrel: New Capabilities and Future Directions," AIAA-2019-0840, January 2019.

[19] Strang, W.Z., Tomaro, R.F. and Grismer, M.J., "The defining methods of Cobalt: a parallel, implicit, unstructured Euler/Navier-Stokes flow solver", AIAA 1999-0786, January 1999.

[20] STAR CCM+ User's Manual 13.06.012-R8, SIEMENS, 2019.

[21] Venkatakrishnan, V., "Convergence to Steady State Solutions of the Euler Equations on Unstructured Grids with Limiters", J. Computational. Phys., Vol. 118, pp120–130, April 1995.

[22] van Leer, B., "Towards the Ultimate Conservative Difference Scheme V. A Second-order Sequel to Godunov's Method", J. Computational Physics, Vol. 32, pp101-136, 1979.

[23] Koren, B., "A robust upwind discretization method for advection, diffusion and source terms", Notes on Numerical Fluid Mechanics, pp117-138, Vieweg, Germany, 1993.

[24] van Albada, G.D., et al., "A Comparative Study of Computational Methods in Cosmic Gas Dynamics", Astronomy and Astrophysics, Vol.108, pp76-84, 1982.

[25] Sweby, P. and Baines, M., "On convergence of Roe's scheme for the general non-linear scalar wave equation", J. Computational Physics, Vol. 56, pp135-148, 1984.

[26] Speigel, S.C., Huyuh, H.T. and DeBonis, J.R., "A survey of the isentropic Euler vortex problem using high-order methods", AIAA 2015-2444, June 2015.